geosciences

MDPI

Article

Impact of Spatial Resolution of Digital Elevation Model on Landslide Susceptibility Mapping: A Case Study in Kullu Valley, Himalayas

Sansar Raj Meena * and Thimmaiah Gudiyangada Nachappa

Department of Geoinformatics—Z_GIS, University of Salzburg, Salzburg 5020, Austria
* Correspondence: sansarraj.meena@sbg.ac.at

Received: 21 July 2019; Accepted: 16 August 2019; Published: 17 August 2019

Abstract: Landslides are one of the most damaging geological hazards in mountainous regions such as the Himalayas. The Himalayan region is, tectonically, the most active region in the world that is highly vulnerable to landslides and associated hazards. Landslide susceptibility mapping (LSM) is a useful tool for understanding the probability of the spatial distribution of future landslide regions. In this research, the landslide inventory datasets were collected during the field study of the Kullu valley in July 2018, and 149 landslide locations were collected as global positioning system (GPS) points. The present study evaluates the LSM using three different spatial resolution of the digital elevation model (DEM) derived from three different sources. The data-driven traditional frequency ratio (FR) model was used for this study. The FR model was used for this research to assess the impact of the different spatial resolution of DEMs on the LSM. DEM data was derived from Advanced Land Observing Satellite-1 (ALOS) Phased Array type L-band Synthetic Aperture Radar (PALSAR) ALOS-PALSAR for 12.5 m, the Advanced Spaceborne Thermal Emission and Reflection Radiometer (ASTER) Global for 30 m, and the Shuttle Radar Topography Mission (SRTM) for 90 m. As an input, we used eight landslide conditioning factors based on the study area and topographic features of the Kullu valley in the Himalayas. The ASTER-Global 30m DEM showed higher accuracy of 0.910 compared to 0.839 for 12.5 m and 0.824 for 90 m DEM resolution. This study shows that that 30 m resolution is better suited for LSM for the Kullu valley region in the Himalayas. The LSM can be used for mitigation and future planning for spatial planners and developmental authorities in the region.

Keywords: natural hazards; landslides; landslide susceptibility mapping (LSM); frequency ratio (FR); ALOS-PALSAR; ASTER; SRTM

1. Introduction

Landslides are one of the most significant geological hazards in mountainous regions all over the world and especially in the Himalayas, where landslides affect the lives of people through damage to property and loss of life [1,2]. One of the most geodynamically active domains is the Himalayas, which is highly susceptible to landslides and other natural hazards [3]. The study area is in the middle Himalayas, positioned in the intercontinental collision zone where the Indian plate is subducting under the Eurasian plate [4]. The Himalayan orogeny that is tectonically the most dynamic mountainous region across the globe is highly vulnerable to landslides and, its associated hazards. The Kullu valley is highly prone to natural hazards, especially landslides in the Himalayas, causing significant damages to the economy [5]. The primary type of landslides in the Kullu valley are rockfalls, rockslides and debris flow, which is of great concern to policymakers, planners and scientists [6]. Historically, the Kullu valley is a popular tourist destination known for landslides and landslides in 1995 caused the death of sixty-five people and destroyed the Kullu town. Landslide susceptibility mapping (LSM)

is usually done by assessing the probability of a landslide occurrence in a given region [7]. Over the years, landslide susceptibility modelling has become a practical approach to obtain better insights into the potential slope failures. Landslide inventory and conditioning factors are required to carry out LSM of an area [8]. The degree of landslide susceptibility of an area is shown as a map, which is the output of LSM. Conditioning factors are essential in LSM as they consider the geological and topographical aspects of the study area. The digital elevation model (DEM) is part of the essential underlying data that is used to derive various significant conditioning factors used in any of the susceptibility analysis for natural hazards. There are various conditioning factors like slope angle, aspect, elevation, plan curvature, topographic roughness index (TRI) and sediment transport index (STI) that can be derived from the DEM based on the assessment criteria and the study area [9]. Various studies have demonstrated the influence of DEM resolution on the quality of the LSM results. However, there is no direct correlation between the resolution of DEM and the quality of the results of the LSM [10–12].

The quality and accuracy of LSM are directly affected by the spatial resolution of the DEM and its derived factors. Much investigation has been carried out in various studies that have investigated the impact of the spatial resolution of conditioning factors on LSM [9,13]. Efforts have been made to understand the effects of landslide conditioning factors on the final susceptibility mapping [14,15]. Depending on the study area, various conditioning factors can be used for carrying out LSM like elevation, altitude, slope angle, plan curvature, rainfall, distance to roads, distance to faults, distance to drainage, geology, lithology and landcover. The most commonly used DEM derived conditioning factors are aspect, slope, elevation, curvature, topographic wetness index (TWI), TRI, and stream power index (SPI) [16–19]. However, fewer studies have explored the effects of the spatial resolution of conditioning factors like DEM on LSM. The researchers in [20] extracted the conditioning factors derived from interferometric synthetic aperture radar (InSAR) data through contour interpolation. They used three different spatial resolution of DEMs, namely 5 m, 10 m, and 25 m, to characterise the relief at different scales for LSM. The study suggested that the DEM resolution is an important criterion and that it can significantly affect the overall accuracy of LSM. They found that results differed between landslide susceptibility classes; however, the higher the DEM spatial resolution, the more strongly the results depended on the valley's topography.

A substantial technical advance has been obtained by presenting algorithms, tools and software to automatically carry out complex tasks such as LSM in short times with robust procedures [21,22]. Also, due to advancements in the geographic information system (GIS) and earth observation technologies, including semi-automatic and machine learning techniques, the preparation of landslide inventory and susceptibility criteria is becoming more attainable and less time-consuming [23,24]. Remote sensing and GIS techniques are considered as the foundations of any natural hazard susceptibility modelling [25]. In the recent years, research has shown that GIS bases statistical models have been used for LSM like logistic regression (LR) [26], random forest (RF) [27], artificial neural networks (ANN) [7], interval pairwise comparison matrices [28], support vector machines (SVM) [29] and the frequency ratio (FR) [30]. In the recent study for the Kullu valley, FR showed greater accuracy compared to the analytical hierarchy process (AHP) along with hybrid spatial multi-criteria [31]. Validation of the various models are to estimate their robustness, prediction skills, and reliability. The most commonly used methods to assess the performance of a model are receiver operating characteristic (ROC), success rate curves, and area under the curve (AUC) [32–35]. There has been no study to assess the impact of DEM on the LSM for the Kullu valley, which is very prone to landslides in India and hence the study area was selected. Thus, this study demonstrates a detailed analysis that shows the impact of DEM resolutions and will contribute to a scientific discussion on this topic.

2. Study Area

The Kullu district is situated in the transitional zone between the lesser and greater Himalayan mountain ranges in the central part of Himachal Pradesh. It has a rugged topography with altitudes ranging from 1300 m to 6000 m above mean sea level with a total area of 1171 km^2 (Figure 1). The study area is characterized by a highly dissected topography, and precipitation amount varies according to the tropical climatic conditions like monsoon season, which has more rainfall compared to the summer season.

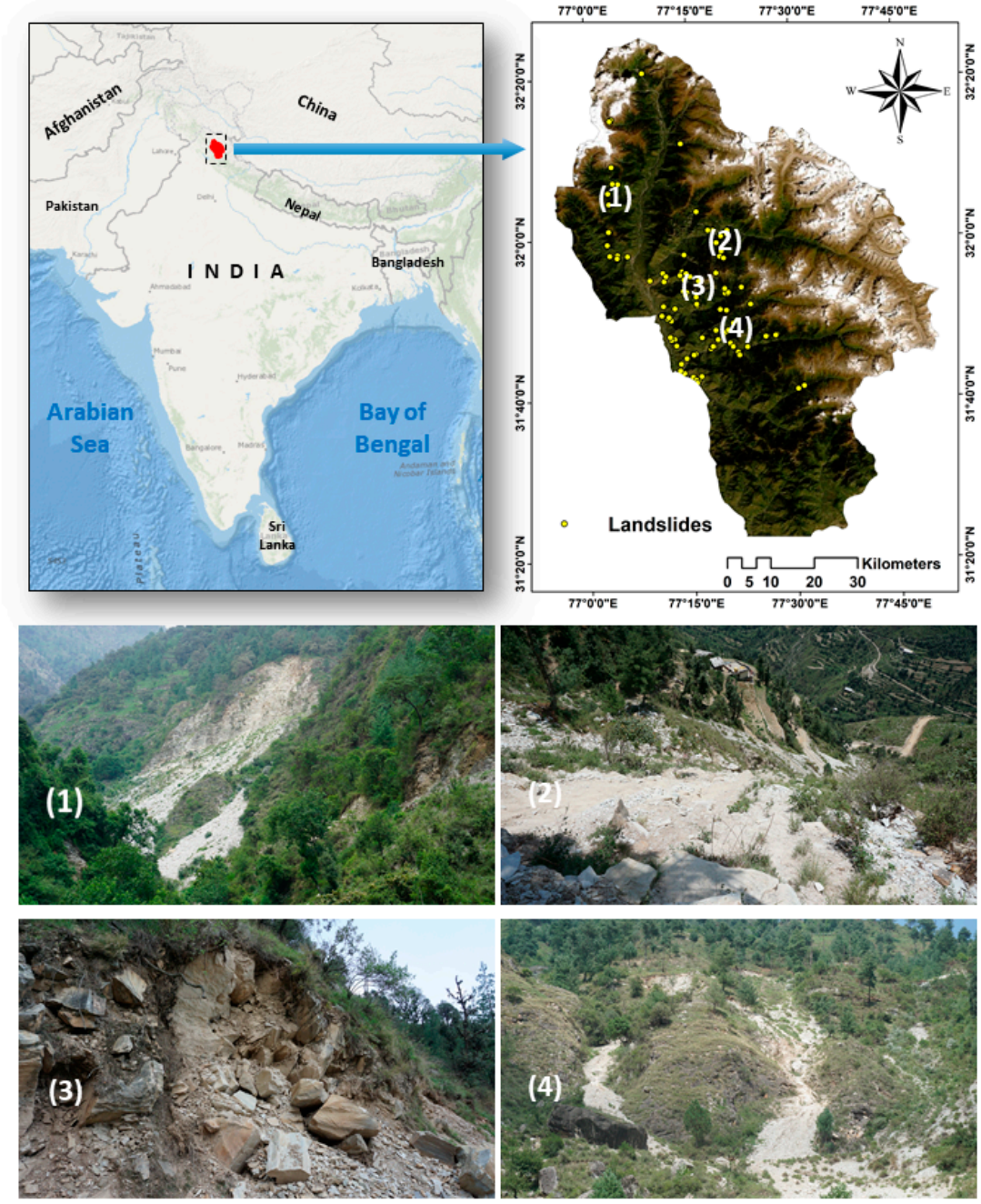

Figure 1. Map shows the location of the study area and the field photographs showing active landslides. (**1**) Phallan (**2**) Jallu (**3**) Kandi (**4**) Devgarh Gohi.

The Beas is the main river in the area. It originates in the Pir-Panjal range, near the Rohtang crest (4038 m), and flows transversally to the two parallel ranges Pir-Panjal and Dhauladhar in the Kullu valley [36]. Typical elevations in the study area range from 1500 m to 6000 m with the highest peak like Manikaran and Sainj reaching almost 6000 m. The higher ranges have magnificent snow-covered peaks and glaciers. From a geomorphic point of view, the Kullu valley is classified into the following nine geomorphic units: Active flood plain, channel island, piedmont slope, river, glaciated terrain, snow cover, younger alluvial plain, highly dissected terrain, moderately dissected terrain, and low dissected terrain. The Kullu valley is characterized by highly variable lithology encompassing of a prevailing congregation of low-to-high-grade meta-sedimentary rocks to diverse lithotectonic groups. As our study area is situated in the Higher Himalayan domain, the geological, structural and climatological settings are favourable for slope deformations. The study area, the Kullu valley, is exposed to a highly dissected topography that is susceptible to heavy rainfall and erosion. The Kullu valley falls in the alpine climate zone, which makes it more prone to frequent landslides. Debris flow is also common as the drainage produces flash floods due to the frequent rainfall.

3. Material and Methods

For this research, we use the FR model to evaluate the effects of different DEM resolutions on the final LSM for Kullu valley. Landslide inventory data from 2014–2017, along with nine conditioning factors, were used for this research. Three different DEM with varying spatial resolution was used for the research that is open and freely available, namely the Advanced Land Observing Satellite-1 (ALOS), the Phased Array type L-band Synthetic Aperture Radar (PALSAR) ALOS-PALSAR for 12.5 m, the Advanced Spaceborne Thermal Emission and Reflection Radiometer (ASTER) Global for 30 m, and the Shuttle Radar Topography Mission (SRTM) for 90 m for the Kullu valley.

3.1. Landslide Inventory

The landslide inventory was created using satellite imagery and field surveys. The foremost step was to identify landslide locations in the satellite imagery and to evaluate landslide-prone areas [23]. Active locations of landslides were mapped, and inventory maps were prepared using various techniques like satellite image interpretation, extensive field survey, and literature searches for historical landslide records [37]. An in-depth field survey was carried out to validate and map the landslides in the study area in July 2018. The landslide inventory illustrates the active landslides along with their properties like the type of landslide, structural attributes and distance from the nearest road. The landslides found in the study area are mainly characterized as debris slides, debris flows and rockfalls based on Varnes classification [38]. Training and testing data are chosen based on the size of the study area, inventory data and the model used. One hundred and forty-nine landslide locations were identified, and these were randomly divided into two groups, with 70% (104) used for training and 30% (#45) for validating the results. This is a standard approach for natural hazard analysis. There are no standard methodologies to assign inventory data for testing and training purpose. Figure 2 shows the distribution of landslide inventory for the study region along with the training and validation datasets.

3.2. Digital Elevation Model (DEM)

Various DEMs, which are available for the Kullu valley in the open data domain, are used to carry out this comparative landslide susceptibility analysis. We used three DEMs of varying spatial resolutions: A 12.5 m DEM from ALOS-PALSAR, a 30 m DEM from ASTER-global and a 90 m DEM from SRTM global. The ASTER scanner, which is installed on the Terra spacecraft of NASA, collects in-track stereo images with two cameras of nadir- and aft-looking near-infrared. Since 2000, these stereo pairs have been used to generate single scenes of 60 × 60 km DEM with vertical accuracies usually between 10 m and 25 m. More common DEMs include the SRTM providing a three arcsec grid, and the Terra ASTER global digital elevation model (GDEM) with a one arcsec grid, which can

provide fundamental topographic information. The high-resolution 12.5 m DEM is a synthetic aperture radar (SAR) interferometry derived DEM, constructed using satellite SAR data from ALOS-PALSAR (radiometrically terrain-corrected, RTC) data downloaded from the Alaska Satellite Facility.

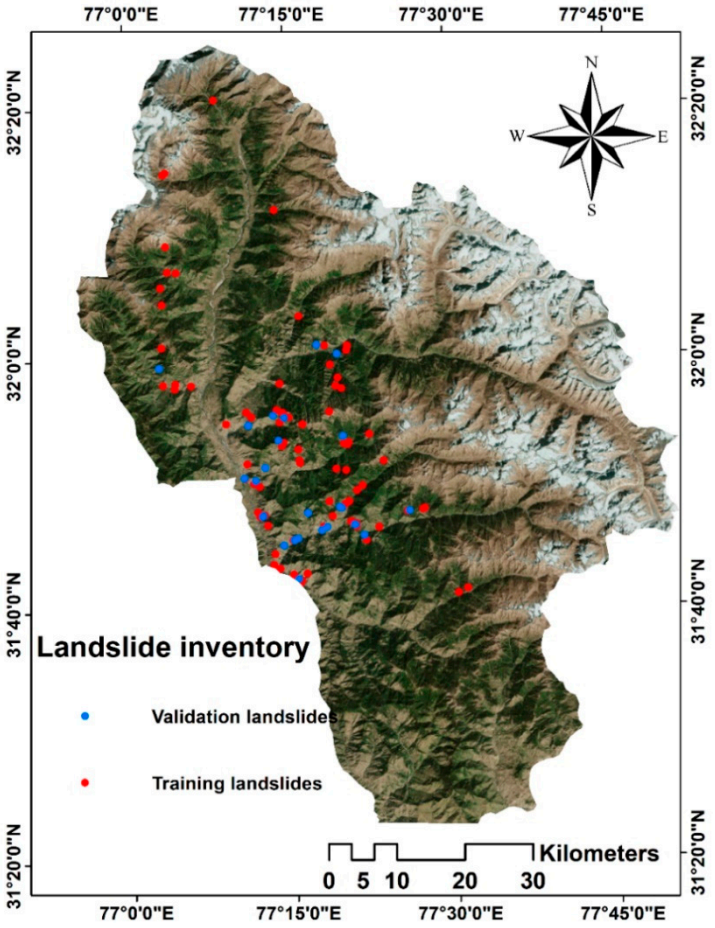

Figure 2. The distribution of landslides for testing and validation in Kullu valley, Himalayas.

3.3. Landslide Conditioning Factors

Eight conditioning factors were selected for the study area based on the topological conditions and availability of the datasets. The conditioning factors were categorized into the four main groups of topographical, geological, hydrological and anthropological. Table 1 shows the categorization of the conditioning factors.

Table 1. Conditioning factors classified based on the main four criteria.

Topographical	Geological	Hydrological	Anthropological
Slope Elevation Aspect	Lithology Distance to Faults	Distance to Drainage	Landforms Distance to Roads

The three different spatial resolution (12.5 m, 30 m and 90 m) DEMs were used for deriving the slope angle, aspect and elevation. The slope angle is one of the most critical factors of the slope stability assessment in any LSM study [39]. The slope angle is directly linked to the landslides, and higher the slope angle is more susceptible to failure. The slope map was divided into five slope categories from 0° to >40° by intervals of 10°.

The elevation is another crucial factor for LSM. Relief classes denote the elevation range from the lowest to the highest point in the study area [40]. The study area was classified into four groups that classified the terrain elevation: 0–1000 m, 1000–3000 m, 3000–4500 m and >4500 m above mean sea level.

The aspect factor impacts the landslide occurrence as this relates to meteorological criteria such as the direction of the precipitation and the amount and frequency of incoming energy and large temperature amplitudes [41]. The aspect factor affects landslides as it relates to meteorological criteria such as precipitation direction and the average amount of sunshine. We classified this aspect into ten classes: North (0°–22.5°; 337.5°–360°), northeast (22.5°–67.5°), east (67.5°–112.5°), southeast (112.5°–157.5°), south (157.5°–202.5°), southwest (202.5°–247.5°), west (247.5°–292.5°), northwest (292.5°–337.5°), north (337.5°–360°) and flat (0°) [31].

Lithology is a crucial factor controlling the landslides as various lithological units have varying geological strength parameters, permeability and susceptibility to failure [42]. There are fourteen lithological units in the stud area, and the layer was prepared based on the quadrangle maps from the Geological Survey of India (GSI) at 1:250,000 scale. The lithological units present in the study area are biotite schist, kynite gneiss; glacio-fluvial deposits; granitic-gneiss and granitoid; micaceous sandstone; pale white to green quartzite; pebbly siltstone; phyllite quartzite, basic flows; quartzite schist; slate phyllite; sreaky banded gneiss; wangtoo granite; phyllite; phyllite schist; purple limestone.

Distance to faults is primarily the causative factor for controlling landslides. Different lithological units and proximity to faults play a significant role in controlling the landslides. Regions that are closer to faults were more affected by earthquakes [43]. The faults were classified, based on the distance to faults, for intervals of 0–500 m, 500–1000 m, 1000–1500 m and >1500 m distance.

Distance to drainage is another major controlling factor for landslide analysis [44]. Drainage provides water that causes material saturation, resulting in landslides in the valleys. The study area was classified into four different buffer ranges. The buffers zones were classified into intervals of 0–100 m, 100–200 m, 200–300 m and >300 m distance.

Landforms classes can differentiate and explain highly dissected zones within the region and the landslide activity that are likely to occur [45]. Kullu valley's landform derived from GSI and was classified into nine landform classes: Younger alluvial plain, highly dissected terrain, the active floodplain, channel island, piedmont slope, river, glaciated terrain, snow cover, moderately dissected terrain, and barely dissected terrain.

Distance to roads is significant for landslide occurrence [4]. The factor was divided into four buffers zones, which signifies the influence of landslides caused by roads. The classes were classified into the interval of buffer zones with 0–50 m, 50–100 m, 100–150 m and >150 m.

All the conditioning factors were classified using ArcGIS software. All the eight conditioning factors was reclassified into three different resolutions for analysis related to the DEM (12.5 m, 30 m and 90 m). For each resolution of DEM, we had eight conditioning factors for analysis using the FR model. Figure 3 shows all the conditioning factors classified for the study area.

Figure 4 shows the total number of landslides in each class of the eight conditioning factors. This also shows that which class is essential for each conditioning factor and how each conditioning factors are classified based on landslide inventory.

3.4. Model Selection

There are various methodologies available like analytical hierarchy process, frequency ratio, support vector machines, random forest, and many others for LSM [46,47]. We chose the FR method as it is directly based on the location of the landslide inventory dataset. This data-driven methodology can clearly illustrate the influence of using DEMs with different resolutions. As the locations of landslides, when represented on different DEM resolutions, will be different in terms of pixel size and cover different areas from the other conditioning factors. In addition, this methodology is considered as of the simplest data-driven methodology that has been used for the LSM in several studies. In the presented

study, we chose FR as we wanted to test if similar outcomes can be obtained with a very simple yet commonly used worldwide LSM method like FR in comparison to more sophisticated methods.

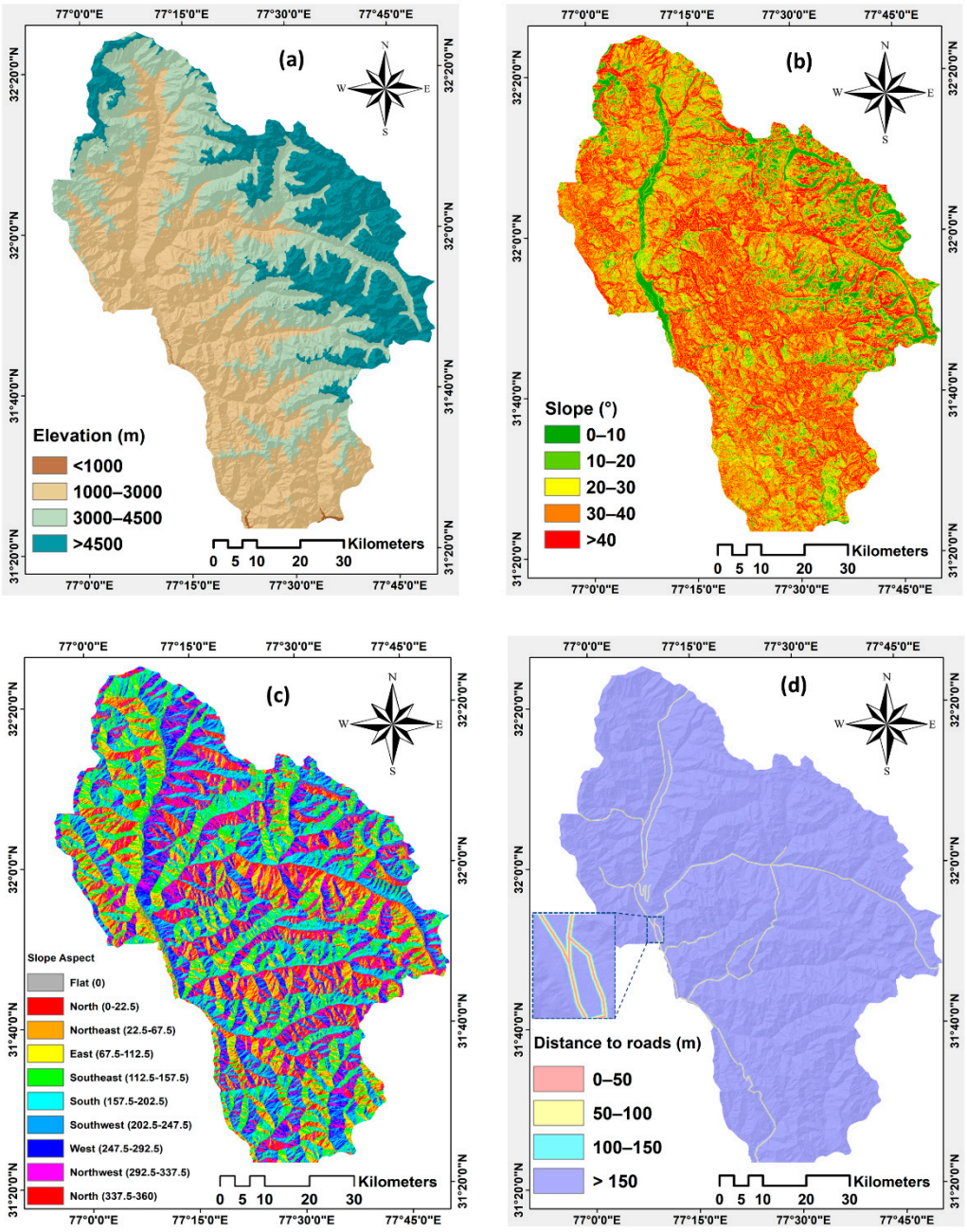

Figure 3. *Cont.*

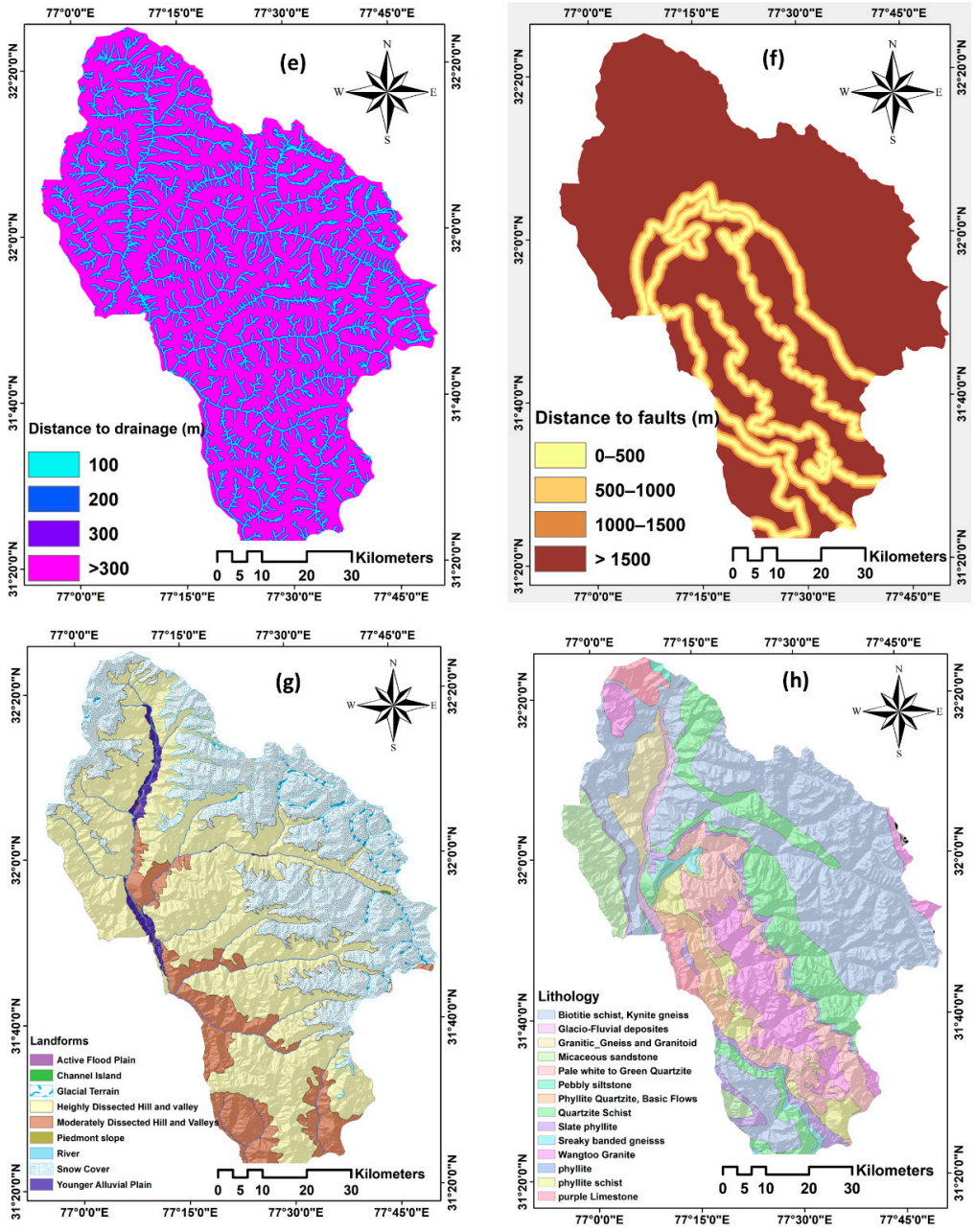

Figure 3. The conditioning factors used in this study are as follows: (**a**) Elevation, (**b**) slope angle, (**c**) slope aspect, (**d**) distance to roads, (**e**) distance to drainage, (**f**) distance to faults, (**g**) landforms, (**h**) lithology.

Frequency Ratio (FR)

The FR model is commonly used for landslide susceptibility analysis [48–50]. This model works based on the ratio of the probability of the landslide occurrence to that of the landslide non-occurrence in a specific area [51,52]. The ratio of the probability can be easily calculated based on the inventory dataset, which is used for obtaining the weight of each class of the criteria [53]. The ratio of the inventory data in each class indicates the significance of the correlation with the landslide susceptibility. A linear combination model (see Equation (1)) can calculate the ratio for different classes of each criterion to the entire considered area:

$$LSM_{FR} = \sum_{i=1}^{n} \sum_{J=1}^{k} FR_{ij}\left[factor_i\left(class_j\right)\right] \quad (1)$$

where n is the number of criteria, and k is the number of classes in each criterion that contributed to the landslide susceptibility map generation. Consequently, FR_{ij} is the FR weight of the jth class in the ith criterion. We used the FR method as this method shows more accurate results for Kullu valley compared to another method like AHP and suited for the study area and hence chose to use this data-driven methodology for the study area.

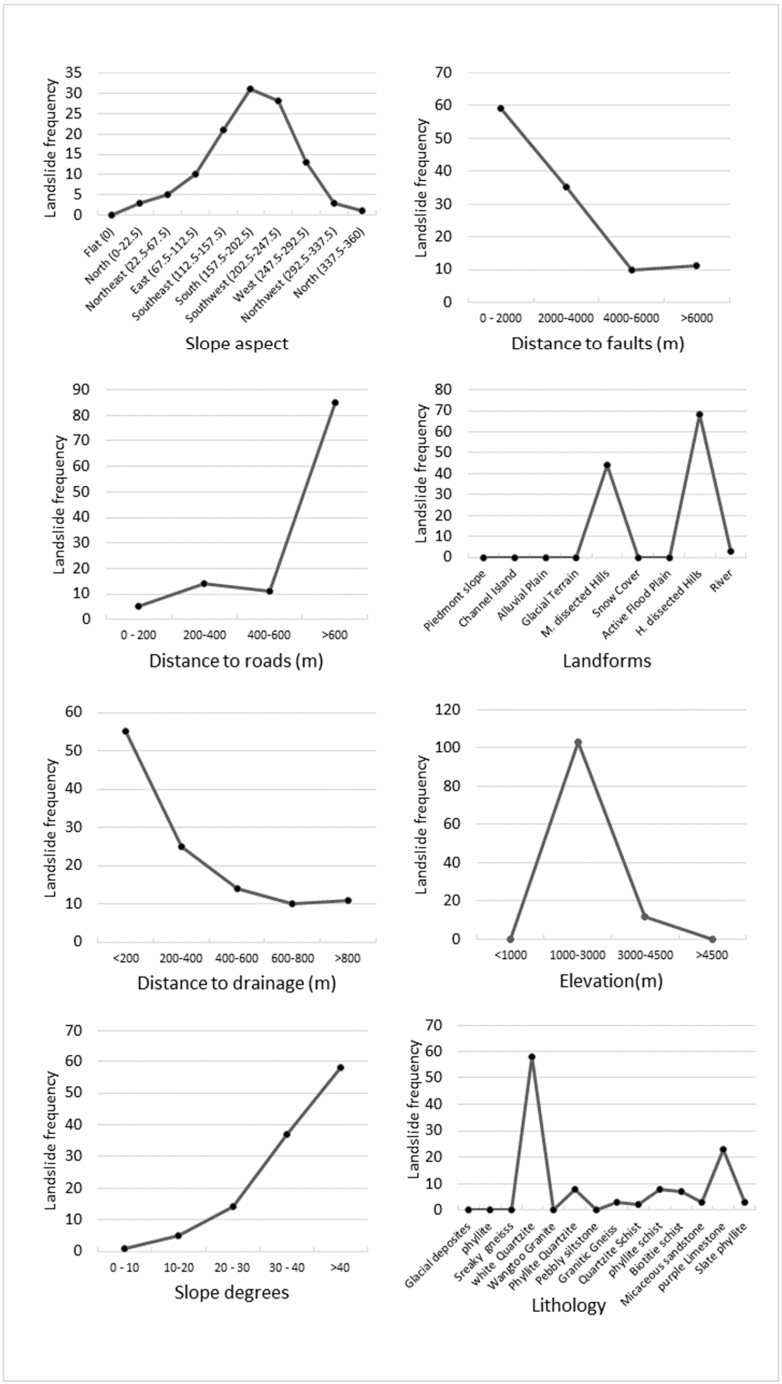

Figure 4. Shows the landslide distribution in each class of the eight conditioning factors.

4. Results

The susceptibility maps were produced using the FR method for three different resolutions. The weights from the FR model was used for the LSM. These LSM were categorised as areas that are highly susceptible to landslides using ArcGIS software. The weights from the FR model for each conditioning factors are represented in Table S1. The derived FR value of over one shows a strong relationship between the landslide data of the training inventory dataset and the high landslide susceptibility class [54]. FR values of less than one show a weak relationship between landslide data of the training inventory dataset and the low landslide susceptibility class.

The resulting landslide susceptibility maps generated based on the three different resolution DEMs (ALOS-PALSAR 12.5 m, ASTER-Global 30 m and SRTM 90 m DEMs) are shown in Figure 5. The natural breaks classification method was used to classify values in the final maps. The susceptibility classes were categorized into five classes from very low, low, moderate, high and very high susceptibility.

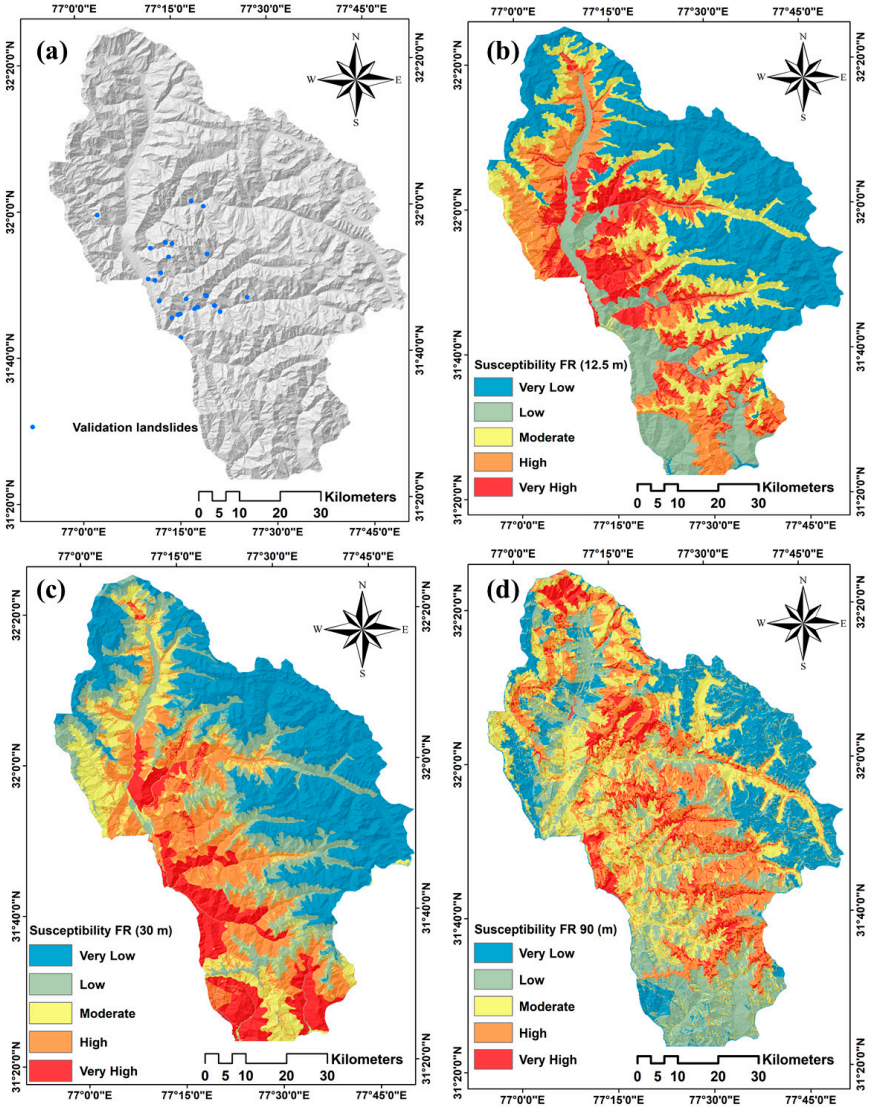

Figure 5. Landslide susceptibility maps resulting from the FR model based on three different resolution DEMs: (**a**) Landslide validation points used for accuracy assessment (**b**) Advanced Land Observing Satellite-1 (ALOS) Phased Array type L-band Synthetic Aperture Radar (PALSAR) (ALOS-PALSAR) 12.5 m, (**c**) Advanced Spaceborne Thermal Emission and Reflection Radiometer (ASTER)-Global 30 m and (**d**) Shuttle Radar Topography Mission (SRTM) 90 m.

5. Validation

The validation section is an essential part of modelling natural hazard susceptibility to predict possible future events [55]. This is a critical process to predict the accuracy of future landslide events. To find the success of the FR model, we use the resulting LSM with the inventory data from the study area. This gives an estimation of the effectiveness of the model used for the LSM and if the model is optimal for the study area and the analysis. In this research, we used 30% (#45) of the landslide inventory for validation. The evaluation of the conformity between landslide inventory data and the resulting susceptibility maps of the applied DEMs can give a clear understanding of the suitability of each resolution of DEM for susceptibility mapping.

5.1. Receiver Operating Characteristics (ROC)

We used receiver operating characteristics (ROC) for validation of the FR model with three different spatial resolution of DEM [56,57]. The ROC approach shows the values between the true positive rate (TPR) and the false positive rate (FPR) in the susceptibility mapping. The y-axis indicates the TPR while the x-axis indicates the FPR. The TPRs are the pixels that are correctly referred to as landslide areas, and FPR are the pixels that are incorrectly referred to as landslide areas [58]. The AUC is the measure which indicates the accuracy of the LSM. The AUC values derived from the ROC approach for three resolution of DEM is 84% for 12.5 m ALOS-PALSAR, 91% for 30 m ASTER-Global and 82% for 90 m SRTM. The validation results showed good agreement between the validation data from the inventory dataset and the resulting susceptibility map from the 30 m resolution DEM from ASTER-Global. The resulting ROC is shown in Figure 6.

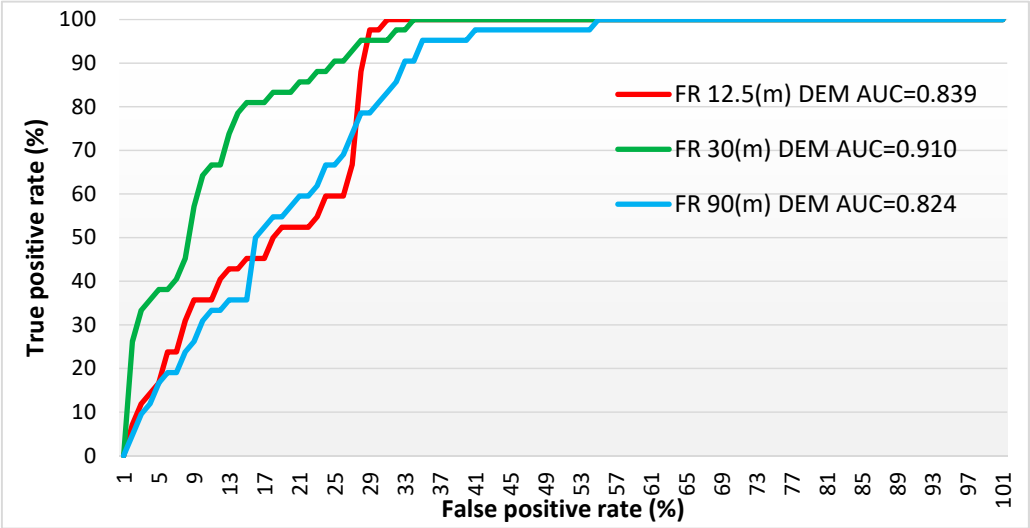

Figure 6. Receiver operating characteristic (ROC) curves representing success rate for the resulting maps from the three different resolution DEMs.

To find the areas that are exposed to landslide susceptibility is critical for spatial managers in order to plan for sustainable risk management and mitigation measures for landslide impacts. This can also save many lives and save the economic damage and loss by protecting the susceptible areas [59].

5.2. Relative Landslide Density (R-index)

R-index is another validation method used mostly in landslide susceptibility analysis. The accuracy of prediction of landslide susceptibility was evaluated using an index of relative landslide density (R-index). We have used 30% (#45) of the total landslide inventory for validation, whereas 70% (#104) of the landslide inventory was used for training. The R-index is given as follows by [60] (see Equation (2)).

$$R = (ni / Ni) / \Sigma(ni / Ni)) \times 100 \quad (2)$$

where ni is the percentage of the area of landslides in each susceptible class and Ni is the percentage of the landslide in each susceptible class [4].

Results show that 30 m DEM has higher R-index values than other two DEM resolutions in very high susceptible classes for both training and testing datasets (See Tables S2 and S3). For the higher landslide susceptibility class, 90 m and 30 m DEMs have comparable R-index values range from 27 to 32 for training and 28 to 30 for testing datasets, which are almost double from 12.5 DEM result. The R-index values show that 30 m DEM resolution has an overall better result than the other two DEM resolution data used in our work (see Figure 7).

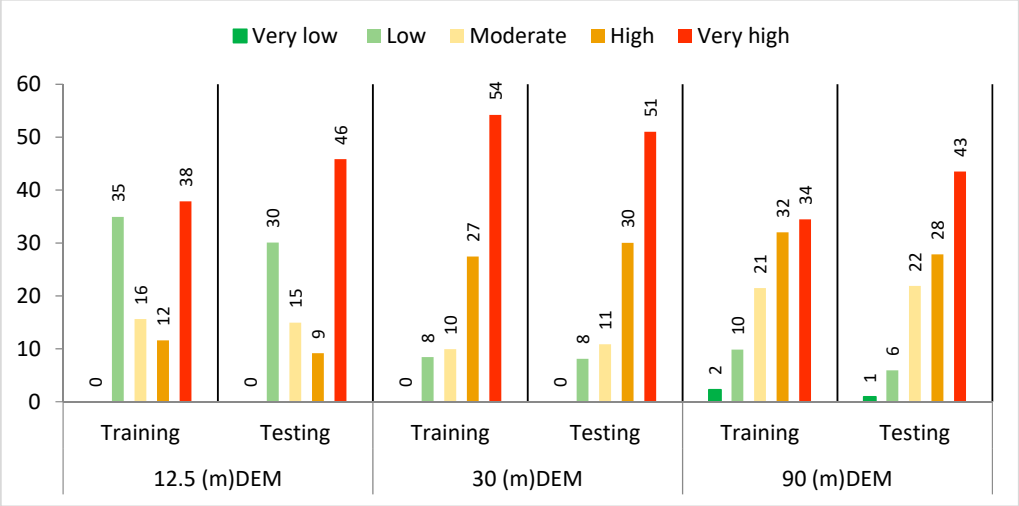

Figure 7. R-index in susceptibility classes for the three different resolution DEMs based on training and testing data.

6. Discussion and Conclusions

The FR model proved to be simple and easy to apply for LSM and suitable for the highly rugged terrain of the Himalayas. This also shows that there is a correlation between landslide distribution and lithological units. Consequently, diverse lithological units display diverse behaviors concerning landslides. In addition, variations in the lithological units and fault lines in the Kullu valley are measured to have a substantial influence on controlling the occurrence of landslides. For the final susceptibility mapping, we used five classes from very low, low, moderate, high and very high using the natural breaks classification. This is a conventional and useful method for classifying landslide susceptibility maps.

For each of the three DEM resolution, we modelled the landslide susceptibility map by analyzing in detail the relevance of the conditioning factors. The analysis is based on landslide inventory data, which was used as empirical input data for the FR model. The results from the AUC and R-index values obtained from the ROC approach shows that DEM derived from ASTER-Global 30 m resolution generated maximum accuracy compared to the much higher spatial resolution DEM of 12.5 m derived from ALOS-PALSAR.

Previous studies have demonstrated the impact of DEM resolution on the output quality of the LSM results showing that there is no correlation between the resolution of DEM and the results. This study also demonstrates that it is not necessary to use conditioning factors with high-resolution for every study area but rather optimal resolution input conditioning factors that are suited to the study area. This also shows that the results in the current research are in line with the previous literature and shows that using higher resolution conditioning factors does not necessarily result in higher accuracy

for the susceptibility map. The limitation of this research is that there was no polygon data available or mapped for this study area for the susceptibility analysis that would have given a better understanding of the model used and the accuracy result. However, as seen in previous studies of LSM, the use of inventory type data (polygon or point) is not so much relevant compared to the impact of DEM resolution [10].

In this research for the Kullu valley, the study shows that 30 m ASTER-Global DEM is best suited for the LSM analysis and subsequently deriving the conditioning factors in the 30 m resolution. These results are better in accuracy than the LSM. This conclusion is based on the current study area and can vary depending on the other study area.

Figure 8 shows the distribution of landslide inventory points in different susceptibility classes in an enlarged sub-area selected from the resulting landslide susceptibility maps. The 12.5 m ALOS-PALSAR and 30 m ASTER-Global show a similar pattern of susceptibility though 12.5 m ALOS-PALSAR shows higher susceptible areas compared to 30 m ASTER-Global and 90 m SRTM. The 90 m SRTM shows a different pattern of susceptibility compared to 12.5 m and 30 m DEM due to the higher spatial resolution, whereas 12.5 m and 30 m DEM show a much better correlation between the susceptibility mappings.

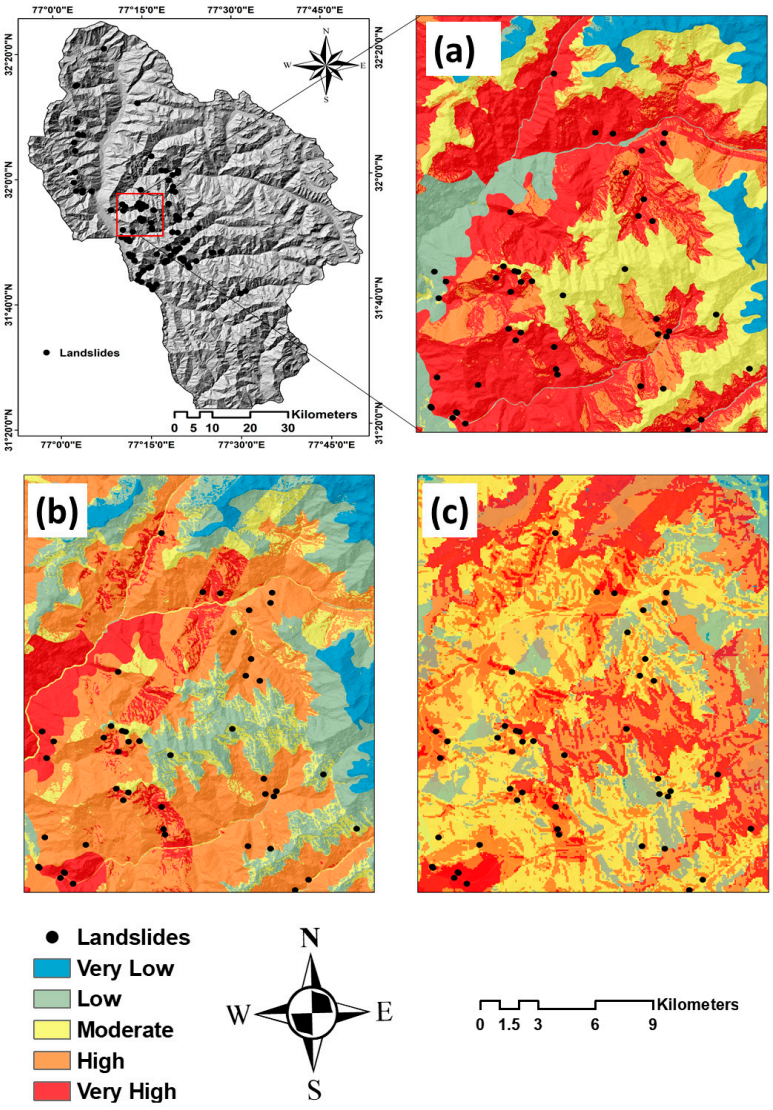

Figure 8. An enlarged sub-area from the resulting landslide susceptibility maps generated based on the three different resolution DEMs: (**a**) 12.5 m DEM, (**b**) 30 m DEM and (**c**) 90 m DEM.

The ASTER-Global 30 m resolution DEM results from FR model is based on the pixels of 30 m resolution, which means a single pixel of factor map represents as the same within the applied pixel size of 30 m resolution. However, when we used the ALOS-PALSAR 12.5 m, each pixel of factor map denotes a 12.5 m resolution. As we applied the point dataset on landslide inventory, the location and area of landslides would be different in various DEM resolutions. Different pixel sizes resulting from different DEM resolutions may cover different areas from the other conditioning factors. All these matters were influenced our resulting LSMs.

The results might differ from one study area to another study area and varies with the topographical conditions of the given study area as well. As the Kullu valley is highly prone to landslides, this study gives the optimal resolution for the FR method. Again, this might differ with other methods as well, and it would be good to continue this study with comparing different models like AHP or spatial multi criteria evaluation (SMCE) or hybrid SMCE to evaluate the impact of DEM resolution on landslide susceptibility.

In future, we aim to develop an object-based LSM approach to evaluate the impact of the different resolution of DEMs. Object-based mapping approach allows defining different sizes of segmentation for further analysis. Further, we would also like to use polygon areas of landslides as the inventory dataset to gain a complete understanding of the impacts of the factor spatial resolution on the LSM process.

Supplementary Materials: The following are available online at http://www.mdpi.com/2076-3263/9/8/360/s1, Table S1: The normalized weights for the classes of the criteria based on the frequency ratio (FR) technique for each digital evaluation model (DEM); Table S2: Resulting R-indexes for the landslide susceptibility mapping (LSMs) based on the three different resolution DEMs for training data; Table S3: Resulting R-indexes for the LSMs based on the three different resolution DEMs for testing data.

Author Contributions: Conceptualization, S.R.M.; methodology, S.R.M.; and T.G.N.; software, S.R.M.; validation, S.R.M.; formal analysis, S.R.M.; data curation, S.R.M.; writing—original draft preparation, S.R.M.; and T.G.N.; writing—review and editing, S.R.M.; and T.G.N.; visualization, S.R.M.; funding acquisition, S.R.M. All authors read and approved the final manuscript.

Funding: Open Access Funding by the University of Salzburg.

Acknowledgments: We would like to thank Anupam Chattopadhyay and Brijendra Kumar Mishra (Department of Geology, University of Delhi, India) for help and support.

Conflicts of Interest: The authors declare no conflict of interest.

References

1. Hölbling, D.; Füreder, P.; Antolini, F.; Cigna, F.; Casagli, N.; Lang, S. A semi-automated object-based approach for landslide detection validated by persistent scatterer interferometry measures and landslide inventories. *Remote Sens.* **2012**, *4*, 1310–1336. [CrossRef]
2. Petley, D. Global patterns of loss of life from landslides. *Geology* **2012**, *40*, 927–930. [CrossRef]
3. Larsen, I.J.; Montgomery, D.R. Landslide erosion coupled to tectonics and river incision. *Nat. Geosci.* **2012**, *5*, 468–473. [CrossRef]
4. Meena, S.; Ghorbanzadeh, O.; Blaschke, T. A comparative study of statistics-based landslide susceptibility models: A case study of the region affected by the gorkha earthquake in nepal. *ISPRS Int. J. Geo Inf.* **2019**, *8*, 94. [CrossRef]
5. Hovland, M.; Gardner, J.V.; Judd, A.G. The significance of pockmarks to understanding fluidflow processes and geohazards. *Geofluids* **2002**, *2*, 127–136. [CrossRef]
6. Varnes, D.J. Slope movement types and processes. *Spec. Rep.* **1978**, *176*, 11–33.
7. Gorsevski, P.V.; Brown, M.K.; Panter, K.; Onasch, C.M.; Simic, A.; Snyder, J. Landslide detection and susceptibility mapping using lidar and an artificial neural network approach: A case study in the cuyahoga valley national park, ohio. *Landslides* **2016**, *13*, 467–484. [CrossRef]
8. Ghorbanzadeh, O.; Feizizadeh, B.; Blaschke, T.; Khosravi, R. Spatially explicit sensitivity and uncertainty analysis for the landslide risk assessment of the gas pipeline networks. In Proceedings of the 21st AGILE Conference on Geo-Information Science, Lund, Sweden, 12–15 June 2018; pp. 1–7.

9. Pradhan, B.; Sameen, M.I. Effects of the spatial resolution of digital elevation models and their products on landslide susceptibility mapping. In *Laser Scanning Applications in Landslide Assessment*; Pradhan, B., Ed.; Springer International Publishing: Cham, Switzerland, 2017; pp. 133–150.
10. Arnone, E.; Francipane, A.; Scarbaci, A.; Puglisi, C.; Noto, L.V. Effect of raster resolution and polygon-conversion algorithm on landslide susceptibility mapping. *Environ. Model. Softw.* **2016**, *84*, 467–481. [CrossRef]
11. Tian, Y.; Xiao, C.; Liu, Y.; Wu, L. Effects of raster resolution on landslide susceptibility mapping: A case study of shenzhen. *Sci. China Ser. E Technol. Sci.* **2008**, *51*, 188–198. [CrossRef]
12. Catani, F.; Lagomarsino, D.; Segoni, S.; Tofani, V. Landslide susceptibility estimation by random forests technique: Sensitivity and scaling issues. *Nat. Hazards Earth Syst. Sci.* **2013**, *13*, 2815–2831. [CrossRef]
13. Chang, K.; Dou, J.; Chang, Y.; Kuo, C.; Xu, K.; Liu, J. Spatial resolution effects of digital terrain models on landslide susceptibility analysis. *ISPRS Int. Ar Chives Photogramm. Remote Sens. Spat. Inf. Sci.* **2016**, *41*, B8.
14. Reichenbach, P.; Rossi, M.; Malamud, B.; Mihir, M.; Guzzetti, F. A review of statistically-based landslide susceptibility models. *Earth Sci. Rev.* **2018**, *180*, 60–91. [CrossRef]
15. Kalantar, B.; Pradhan, B.; Naghibi, S.A.; Motevalli, A.; Mansor, S. Assessment of the effects of training data selection on the landslide susceptibility mapping: A comparison between support vector machine (svm), logistic regression (lr) and artificial neural networks (ann). *Geomatics Nat. Hazards Risk* **2018**, *9*, 49–69. [CrossRef]
16. Aghda, S.F.; Bagheri, V.; Razifard, M. Landslide susceptibility mapping using fuzzy logic system and its influences on mainlines in lashgarak region, tehran, iran. *Geotech. Geol. Eng.* **2018**, *36*, 915–937.
17. Akgün, A.; Bulut, F. Gis-based landslide susceptibility for arsin-yomra (trabzon, north turkey) region. *Environ. Geol.* **2007**, *51*, 1377–1387. [CrossRef]
18. Chen, W.; Sun, Z.; Han, J. Landslide susceptibility modeling using integrated ensemble weights of evidence with logistic regression and random forest models. *Appl. Sci.* **2019**, *9*, 171. [CrossRef]
19. Pradhan, B. Landslide susceptibility mapping of a catchment area using frequency ratio, fuzzy logic and multivariate logistic regression approaches. *J. Indian Soc. Remote Sens.* **2010**, *38*, 301–320. [CrossRef]
20. Schlögel, R.; Marchesini, I.; Alvioli, M.; Reichenbach, P.; Rossi, M.; Malet, J.P. Optimizing landslide susceptibility zonation: Effects of dem spatial resolution and slope unit delineation on logistic regression models. *Geomorphology* **2018**, *301*, 10–20. [CrossRef]
21. Akgun, A.; Sezer, E.A.; Nefeslioglu, H.A.; Gokceoglu, C.; Pradhan, B. An easy-to-use matlab program (mamland) for the assessment of landslide susceptibility using a mamdani fuzzy algorithm. *Comput. Geosci.* **2012**, *38*, 23–34. [CrossRef]
22. Lagomarsino, D.; Tofani, V.; Segoni, S.; Catani, F.; Casagli, N. A tool for classification and regression using random forest methodology: Applications to landslide susceptibility mapping and soil thickness modeling. *Environ. Modeling Assess.* **2017**, *22*, 201–214. [CrossRef]
23. Ghorbanzadeh, O.; Blaschke, T.; Gholamnia, K.; Meena, S.R.; Tiede, D.; Aryal, J. Evaluation of different machine learning methods and deep-learning convolutional neural networks for landslide detection. *Remote Sens.* **2019**, *11*, 196. [CrossRef]
24. Ghorbanzadeh, O.; Blaschke, T. Optimizing sample patches selection of cnn to improve the miou on landslide detection. In Proceedings of the 5th International Conference on Geographical Information Systems Theory, Applications and Management: GISTAM 2019, Heraklion, Greece, 3–5 May 2019; p. 8.
25. Hölbling, D.; Spiekermann, R.; Betts, H.; Phillips, C. Landslide Hotspot Mapping and Susceptibility Assessment in Pahiatua, New Zealand. In Proceedings of the EGU General Assembly Conference Abstracts, Vienna, Austria, 8–13 April 2018; p. 4214.
26. Pourghasemi, H.; Gayen, A.; Park, S.; Lee, C.-W.; Lee, S. Assessment of landslide-prone areas and their zonation using logistic regression, logitboost, and naïvebayes machine-learning algorithms. *Sustainability* **2018**, *10*, 3697. [CrossRef]
27. Brenning, A. Spatial prediction models for landslide hazards: Review, comparison and evaluation. *Nat. Hazards Earth Syst. Sci.* **2005**, *5*, 853–862. [CrossRef]
28. Feizizadeh, B.; Ghorbanzadeh, O. Gis-based interval pairwise comparison matrices as a novel approach for optimizing an analytical hierarchy process and multiple criteria weighting. *GI_Forum* **2017**, *1*, 27–35. [CrossRef]

29. Bui, D.T.; Tuan, T.A.; Klempe, H.; Pradhan, B.; Revhaug, I. Spatial prediction models for shallow landslide hazards: A comparative assessment of the efficacy of support vector machines, artificial neural networks, kernel logistic regression, and logistic model tree. *Landslides* **2016**, *13*, 361–378.
30. Demir, G.; Aytekin, M.; Akgün, A.; Ikizler, S.B.; Tatar, O. A comparison of landslide susceptibility mapping of the eastern part of the north anatolian fault zone (turkey) by likelihood-frequency ratio and analytic hierarchy process methods. *Nat. Hazards* **2013**, *65*, 1481–1506. [CrossRef]
31. Meena, S.R.; Mishra, B.K.; Tavakkoli Piralilou, S. A hybrid spatial multi-criteria evaluation method for mapping landslide susceptible areas in kullu valley, himalayas. *Geosciences* **2019**, *9*, 156. [CrossRef]
32. Yan, F.; Zhang, Q.; Ye, S.; Ren, B. A novel hybrid approach for landslide susceptibility mapping integrating analytical hierarchy process and normalized frequency ratio methods with the cloud model. *Geomorphology* **2019**, *327*, 170–187. [CrossRef]
33. Chen, W.; Panahi, M.; Tsangaratos, P.; Shahabi, H.; Ilia, I.; Panahi, S.; Li, S.; Jaafari, A.; Ahmad, B.B. Applying population-based evolutionary algorithms and a neuro-fuzzy system for modeling landslide susceptibility. *Catena* **2019**, *172*, 212–231. [CrossRef]
34. Zhang, T.; Han, L.; Chen, W.; Shahabi, H. Hybrid integration approach of entropy with logistic regression and support vector machine for landslide susceptibility modeling. *Entropy* **2018**, *20*, 884. [CrossRef]
35. Linden, A. Measuring diagnostic and predictive accuracy in disease management: An introduction to receiver operating characteristic (roc) analysis. *J. Eval. Clin. Pract.* **2006**, *12*, 132–139. [CrossRef] [PubMed]
36. Meena, S.R.; Mishra, B.K. Landslide risk assessment of kullu valley using frequency ratio methods and its controlling mechanism, himachal himalayas, india. In Proceedings of the INQUIMUS 2018 Workshop "Methods and Tools to Assess Multi-Hazard Risk, Vulnerability and Resilience", Venice, Italy, 3–5 December 2018.
37. Pisano, L.; Zumpano, V.; Malek, Z.; Rosskopf, C.M.; Parise, M. Variations in the susceptibility to landslides, as a consequence of land cover changes: A look to the past, and another towards the future. *Sci. Total Environ.* **2017**, *601*, 1147–1159. [CrossRef]
38. Cruden, D.M.; Varnes, D.J. Landslide types and processes, special report, transportation research board, national academy of sciences. *Spec. Rep. Natl. Res. Counc. Transp. Res. Board* **1996**, *247*, 76.
39. Feizizadeh, B.; Roodposhti, M.S.; Jankowski, P.; Blaschke, T. A gis-based extended fuzzy multi-criteria evaluation for landslide susceptibility mapping. *Comput. Geosci.* **2014**, *73*, 208–221. [CrossRef]
40. Raja, N.B.; Įiįek, I.; Türkoğlu, N.; Aydin, O.; Kawasaki, A. Correction to: Landslide susceptibility mapping of the sera river basin using logistic regression model. *Nat. Hazards* **2018**, *91*, 1423. [CrossRef]
41. Felicísimo, Á.M.; Cuartero, A.; Remondo, J.; Quirós, E. Mapping landslide susceptibility with logistic regression, multiple adaptive regression splines, classification and regression trees, and maximum entropy methods: A comparative study. *Landslides* **2013**, *10*, 175–189. [CrossRef]
42. Mishra, B.K.; Bhattacharjee, D.; Chattopadhyay, A.; Prusty, G. Tectonic and lithologic control over landslide activity within the larji–kullu tectonic window in the higher himalayas of india. *Nat. Hazards* **2018**, *92*, 673–697. [CrossRef]
43. Chen, W.; Pourghasemi, H.R.; Naghibi, S.A. A comparative study of landslide susceptibility maps produced using support vector machine with different kernel functions and entropy data mining models in china. *Bull. Eng. Geol. Environ.* **2017**, *77*, 647–664. [CrossRef]
44. Gokceoglu, C.; Sonmez, H.; Nefeslioglu, H.A.; Duman, T.Y.; Can, T. The 17 march 2005 kuzulu landslide (sivas, turkey) and landslide-susceptibility map of its near vicinity. *Eng. Geol.* **2005**, *81*, 65–83. [CrossRef]
45. Pourghasemi, H.; Pradhan, B.; Gokceoglu, C.; Moezzi, K.D. Landslide susceptibility mapping using a spatial multi criteria evaluation model at haraz watershed, iran. In *Terrigenous Mass Movements*; Springer: Berlin/Heidelberg, Germany, 2012; pp. 23–49.
46. Choubin, B.; Moradi, E.; Golshan, M.; Adamowski, J.; Sajedi-Hosseini, F.; Mosavi, A. An ensemble prediction of flood susceptibility using multivariate discriminant analysis, classification and regression trees, and support vector machines. *Sci. Total Environ.* **2019**, *651*, 2087–2096. [CrossRef] [PubMed]
47. Meena, S.R.; Ghorbanzadeh, O.; Hölbling, D.; Albrecht, F.; Blaschke, T. A conceptual framework for web-based nepalese landslide information system. *Nat. Hazards Earth Syst. Sci. Discuss.* **2019**, *2019*, 1–20. [CrossRef]
48. Wang, Q.; Li, W. A gis-based comparative evaluation of analytical hierarchy process and frequency ratio models for landslide susceptibility mapping. *Phys. Geogr.* **2017**, *38*, 318–337. [CrossRef]

49. Hong, H.; Chen, W.; Xu, C.; Youssef, A.M.; Pradhan, B.; Tien Bui, D. Rainfall-induced landslide susceptibility assessment at the chongren area (china) using frequency ratio, certainty factor, and index of entropy. *Geocarto Int.* **2017**, *32*, 139–154. [CrossRef]
50. Mondal, S.; Maiti, R. Integrating the analytical hierarchy process (ahp) and the frequency ratio (fr) model in landslide susceptibility mapping of shiv-khola watershed, darjeeling himalaya. *Int. J. Disaster Risk Sci.* **2013**, *4*, 200–212. [CrossRef]
51. Bonham-Carter, G.F. Geographic information systems for geoscientists-modeling with gis. *Comput. Methods Geosci.* **1994**, *13*, 398.
52. Park, S.; Choi, C.; Kim, B.; Kim, J. Landslide susceptibility mapping using frequency ratio, analytic hierarchy process, logistic regression, and artificial neural network methods at the inje area, korea. *Environ. Earth Sci.* **2013**, *68*, 1443–1464. [CrossRef]
53. Shahabi, H.; Hashim, M. Landslide susceptibility mapping using gis-based statistical models and remote sensing data in tropical environment. *Sci. Rep.* **2015**, *5*, 9899. [CrossRef]
54. Shahabi, H.; Hashim, M.; Ahmad, B.B. Remote sensing and gis-based landslide susceptibility mapping using frequency ratio, logistic regression, and fuzzy logic methods at the central zab basin, iran. *Environ. Earth Sci.* **2015**, *73*, 8647–8668. [CrossRef]
55. Ghorbanzadeh, O.; Rostamzadeh, H.; Blaschke, T.; Gholaminia, K.; Aryal, J. A new gis-based data mining technique using an adaptive neuro-fuzzy inference system (anfis) and k-fold cross-validation approach for land subsidence susceptibility mapping. *Nat. Hazards* **2018**, *94*, 497–517. [CrossRef]
56. Ghorbanzadeh, O.; Blaschke, T. Wildfire susceptibility evaluation by integrating an analytical network process approach into gis-based analyses. *Int. J. Adv. Sci. Eng. Technol.* **2018**, *6*, 48–53.
57. Ghorbanzadeh, O.; Valizadeh Kamran, K.; Blaschke, T.; Aryal, J.; Naboureh, A.; Einali, J.; Bian, J. Spatial prediction of wildfire susceptibility using field survey gps data and machine learning approaches. *Fire* **2019**, *2*, 43. [CrossRef]
58. Ghorbanzadeh, O.; Blaschke, T.; Aryal, J.; Gholaminia, K. A new gis-based technique using an adaptive neuro-fuzzy inference system for land subsidence susceptibility mapping. *J. Spat. Sci.* **2018**, *21*, 1–17. [CrossRef]
59. Nsengiyumva, J.B.; Luo, G.; Nahayo, L.; Huang, X.; Cai, P. Landslide susceptibility assessment using spatial multi-criteria evaluation model in rwanda. *Int. J. Environ. Res. Public Health* **2018**, *15*, 243. [CrossRef] [PubMed]
60. Baeza, C.; Corominas, J. Assessment of shallow landslide susceptibility by means of multivariate statistical techniques. *Earth Surf. Process. Landf.* **2001**, *26*, 1251–1263. [CrossRef]